

Supplementary Material for

In-Cloud Oxalate Formation in the Global Troposphere: A 3D Modeling Study

S. Myriokefalitakis^{1,2}, K. Tsigaridis^{3,4}, N. Mihalopoulos¹, J. Sciare⁵, A. Nenes^{6,7,2}, K. Kawamura⁸, A. Segers⁹ and M. Kanakidou¹

¹Environmental Chemical Processes Laboratory, Department of Chemistry, University of Crete, 71003, P.O. Box 2208, Heraklion, Greece

²Institute of Chemical Engineering and High Temperature Chemical Processes (ICE-HT), Foundation for research and Technology Hellas (FORTH), 26504 Patras, Greece

³Center for Climate Systems Research, Columbia University, New York, NY 10025, USA

⁴NASA Goddard Institute for Space Studies, New York, NY 10025, USA

⁵Laboratoire des Sciences du Climat et de l'Environnement (LSCE), CNRS/CEA, 91190 Gif sur Yvette, France

⁶School of Earth and Atmospheric Sciences, Georgia Institute of Technology, 311 Ferst Drive, Atlanta, GA 30332-0100, USA

⁷School of Chemical and Biomolecular Engineering, Georgia Institute of Technology, 311 Ferst Drive, Atlanta, GA 30332-0100, USA

⁸Institute of Low Temperature Science, Hokkaido University, Sapporo, Japan

⁹TNO Built Environment and Geosciences, Department of Air Quality and Climate, P.O. Box 80015, 3508 TA Utrecht, The Netherlands

Correspondence to: M. Kanakidou (mariak@chemistry.uoc.gr)

Supplementary Tables:

Table S1. Aqueous phase equilibrium used in TM4-ECPL. Dissociation constants are taken from Lim et al. (2005) unless referred differently. Dissociation constants are expressed in mol L⁻¹ and are calculated as follows:

$$k^{eq} = k_{298}^{eq} \exp \left[-\frac{\Delta H}{R} \left(\frac{1}{T} - \frac{1}{298} \right) \right]$$

<i>Aqueous Phase Equilibrium</i>			k_{298}^{eq}	$-\frac{\Delta H}{R}$
H ₂ O	\leftrightarrow	HO ⁻ + H ⁺	1.0 10 ⁻¹⁴	-6716
HO ₂	\leftrightarrow	O ₂ ⁻ + H ⁺	3.5 10 ⁻⁵ ^a	
H ₂ O ₂	\leftrightarrow	HO ₂ ⁻ + H ⁺	2.2 10 ⁻¹² ^a	-3730
SO ₂ .H ₂ O	\leftrightarrow	HSO ₃ ⁻ + H ⁺	1.3 10 ⁻² ^a	1960
HSO ₃ ⁻	\leftrightarrow	SO ₃ ²⁻ + H ⁺	6.6 10 ⁻⁸ ^a	1500
HNO ₃	\leftrightarrow	NO ₃ ⁻ + H ⁺	2.2 10 ¹	1800
NH ₃ .H ₂ O	\leftrightarrow	NH ₄ ⁺ + HO ⁻	1.77 10 ⁻⁵	-560
CO ₂ .H ₂ O	\leftrightarrow	HCO ₃ ⁻ + H ⁺	4.3 10 ⁻⁷	-913
HCO ₃ ⁻	\leftrightarrow	CO ₃ ²⁻ + H ⁺	4.69 10 ⁻¹¹	-1820
HCOOH	\leftrightarrow	HCOO ⁻ + H ⁺	1.77 10 ⁻⁴	12
CH ₃ COOH	\leftrightarrow	CH ₃ COO ⁻ + H ⁺	1.75 10 ⁻⁵	46
PRV	\leftrightarrow	PRV ⁻ + H ⁺	3.2 10 ⁻³	
GLX	\leftrightarrow	GLX ⁻ + H ⁺	3.47 10 ⁻⁴	-267
OXL	\leftrightarrow	OXL ⁻ + H ⁺	5.6 10 ⁻³	-453
OXL ⁻	\leftrightarrow	OXL ²⁻ + H ⁺	5.42 10 ⁻⁵	-805

^a Seinfeld and Pandis (1998)

Table S2. Effective Henry's law constants for pure water used in TM4-ECPL. Effective Henry constants are taken from Sander (1999) unless referred differently. Effective Henry constants are expressed in mol L⁻¹ atm⁻¹ and are calculated as follows:

$$H^{eff} = H_{298}^{eff} \exp \left[-\frac{\Delta H}{R} \left(\frac{1}{T} - \frac{1}{298} \right) \right]$$

<i>Species</i>	H_{298}^{eff}	$-\frac{\Delta H}{R}$
O ₃	1.3 10 ⁻²	2000
OH	3.0 10 ¹	4500
HO ₂	4.6 10 ³	4800
H ₂ O ₂	8.6 10 ⁴	6500
NO ₃	2.0	2000
HNO ₃	2.4 10 ⁶	8700
SO ₂	1.4	2800
NH ₃	6.1 10 ¹	4200
CO ₂	3.5 10 ⁻²	2400
HCHO	3.2 10 ³	6800
GLYAL	4.1 10 ⁴	4600
GLY ^a	4.19 10 ⁵	62200/R
MGLY	3.7 10 ³	7500
HCOOH	8.9 10 ³	6100
CH ₃ COOH	4.1 10 ³	6300
PRV	3.1 10 ⁵	5100
GLX ^a	1.09 10 ⁴	40000/R
OXL ^b	3.26 10 ⁶	

^a Ip et al. (2009); R=8.314 J mol⁻¹ K⁻¹ is the universal gas constant

^b Brimblecombe et al. (1992); The temperature dependence effective Henry's value is calculated as $\ln(H^{eff}) = -9.45 + 7285/T$

Table S3. Location of stations with OXL observations, time, station classification, concentrations (in ng m⁻³) and analytical method taken into account for the model validation in Fig. 6.

Location	Time	Station Classification	Measurements	Filters	Analytical Method	Reference
California, USA	June – September, 1984	Urban - Surface	490	Quartz	GC-MS	Kawamura et al., 1985
Monterey, CA	24 August – 3 September, 2002	Urban - Air	140±30	#PTFE	IC	Crahan et al., 2004
Mexico City, Mexico	17-30 March, 2006	Urban - Surface	1330±620	Quartz	HPLC-MS/MS	Stone et al., 2010
Chicago, USA	July-August, 2002 and July, 2003 11-19	Urban - Surface	118±0	Quartz	IC	Fosco and Schmeling, 2006
Claremont, CA	September, 1985	Urban - Surface	210	Nylon-Nylon	IC	Grosjean, 1988
Sao Paulo, Brazil	July, 1996 16-18	Urban - Surface	1140±1200	PTFE	IC	Souza et al., 1999
Vienna, Austria	February, 1999	Urban - Surface	86±25	Quartz	GC/MS	Limbeck et al., 2005
Vienna, Austria	June, 1997	Urban - Surface	340	Quartz	GC-FID-MS	Limbeck and Puxbaum, 1999
Lahore, Pakistan	December, 2005 – February, 2006 10-15	Urban - Surface	600±520	PTFE	IC	Biswas et al., 2008
Baoji, China	February, 2008	Urban - Surface	816±172	Quartz	GC-MS	Wang et al., 2010
Baoji, China	1-6 April, 2008	Urban - Surface	532±247	Quartz	GC-MS	Wang et al., 2010
Tokyo, Japan	April, 1988 – February, 1989 24-26	Urban - Surface	270±190	Quartz	GC-MS	Kawamura and Ikushima, 1993
Tokyo, Japan	February, 1992	Urban - Surface	521-650	Quartz	GC-MS	Sempere and Kawamura, 1994
Tokyo, Japan	22-23 July, 1992	Urban - Surface	1352-1680	Quartz	GC-MS	Sempere and Kawamura, 1994
Helsinki, Finland	April-May, 2006	Urban - Surface	91±110	Quartz	IC	Saarnio et al., 2010
Helsinki, Finland	July and September, 2006 23 -28	Urban - Surface	50±37	Quartz	IC	Saarnio et al., 2010
Chennai, India	January, 2007 November 2006– February 2007	Urban - Surface	472.4±136.9	Quartz	GC-MS	Pavuluri et al., 2010
New Delhi, India	July and February 2007	Urban - Surface	1431 (396–4531)	Quartz	GC	Miyazaki et al., 2009
Denver, USA	August, 1981 and 1982 July and September, 2003	Rural - Surface	<180	PTFE	IC	Norton et al., 1993
N. Carolina, USA	September, 2003	Rural - Surface	10-200	PTFE	IC	Lewandowski et al., 2007

<i>Location</i>	<i>Time</i>	<i>Station Classification</i>	<i>Measurements</i>	<i>Filters</i>	<i>Analytical Method</i>	<i>Reference</i>
Sydney, FL	27 April - 31 May, 2002	Rural - Surface	290	Glass fiber	IC	Martinelango et al., 2006
Amazon Basin, Brazil	July-August, 1985	Rural - Air	158±59	PTFE	IC	Talbot et al., 1988
Rondonia, Brazil	8 September - 11 November, 2002	Rural - Surface	22-1340	Quartz-PTFE	IC	Falkovich et al., 2005
Rondonia, Brazil	1 September- 25 October, 1999 16- 26	Rural - Surface	1356 (695-2059)	Quartz	GC	Kundu et al., 2010
Rondonia, Brazil	September, 2002	Rural - Surface	140-1330	Quartz	IC	Graham et al., 2002
*Aveiro, Portugal	July, 2002 – June, 2004	Rural - Surface	262±117	Quartz	IC	Legand et al., 2007 / CARBOSOL consortium
*Puy de Dome, France	September, 2002 - September, 2004	Rural - Surface	137±85	Quartz	IC	Legand et al., 2007 / CARBOSOL consortium
*Schauinland, Germany	October, 2002 – September, 2004	Rural - Surface	223±105	Quartz	IC	Legand et al., 2007 / CARBOSOL consortium
*K-Pustza, Hungary	July, 2002 – May, 2004	Rural - Surface	288±93	Quartz	IC	Legand et al., 2007 / CARBOSOL consortium
Goldlauter, Germany	7-8 and 26-27 October, 2001	Rural - Surface	>104	Quartz	GC-MS	Muller et al., 2005
Fichtelgebirge, Germany	July, 2002	Rural - Surface	69±19	Quartz	GC-MS	Plewka et al., 2006
Salzburg, Austria	July, 2002	Rural - Surface	153	Quartz	GC-MS	Limbeck and Puxbaum, 1999
Nylsvley, South Africa	May, 1997	Rural - Surface	193	Quartz	GC-MS	Limbeck and Puxbaum, 1999
Mt. Rax, Austria	12–25 April, 1999	Rural - Surface	57±32	Quartz	GC-MS	Limbeck et al., 2005
Bangui, Central Africa	November, 1996	Rural - Surface	140±50	Glass fiber	IC	Ruellan et al., 1999
Valencia, Spain	11 September - 19 October, 2006	Rural - Surface	200 (100-400)	Quartz	IC	Vianna et al., 2008
Mount Tai, China	22–28 June, 2006	Rural - Surface	365±85	Quartz	GC/FID	Wang et al., 2009
Mangshan, China	15 September - 5 October, 2007	Rural - Surface	760	Quartz	GC	He and Kawamura, 2010
*Mace Head, Ireland	April– September, 1998	Marine - Surface	101±47	Quartz	CE	Kleefeld et al., 2002
*Alert, Canada	22 January - 20 April, 1992	Marine - Surface	27 (7-65)	Quartz	GC/MS	Kawamura et al., 2005
Azores, Terceira Island	October, 1998 – March, 1999	Marine - Surface	54±27	Quartz	IC	Legand et al., 2007 / CARBOSOL consortium
*Finokalia, Greece	January - December, 2005	Marine - Surface	155±60	PTFE	IC	Mihalopoulos, N., 2011, pers. com.

<i>Location</i>	<i>Time</i>	<i>Station Classification</i>	<i>Measurements</i>	<i>Filters</i>	<i>Analytical Method</i>	<i>Reference</i>
*Amsterdam Island	May, 2003 - December, 2004	Marine - Surface	11.3±2.2	Quartz	IC	Sciare, J, 2011, pers. com
Syowa Station, Antarctica	19 March -29 April, 1991	Marine - Surface	1.59	Quartz	GC	Kawamura et al., 1996
Syowa Station, Antarctica	13 May - 9 June, 1991	Marine - Surface	3.12	Quartz	GC	Kawamura et al., 1996
Syowa Station, Antarctica	29 August – 29 October, 1991	Marine - Surface	3.26	Quartz	GC	Kawamura et al., 1996
Syowa Station, Antarctica	28 November – 31 December, 1991	Marine - Surface	10.29	Quartz	GC	Kawamura et al., 1996
Indian Ocean - Arabian Sea	February – March, 1999	Marine - Ship	103±62	Quartz	GC/MS	Neussus et al., 2002
Jesu Island, Korea	13 - 29 April, 2001	Marine - Surface	430±290	PTFE	IC	Topping et al., 2004
Jesu Island, Korea	April, 2003 – April, 2004	Marine - Surface	458 (92-1293)	Quartz	GC	Kundu et al., 2010
Atlantic Ocean	11 October – 2 November, 1996	Marine - Ship	46±43	PTFE	IC	Baboukas et al., 2000
North Pacific Ocean	29 July - 19 August, 2008	Marine - Ship	47±18	Quartz	GC	Miyazaki et al., 2010

*Monthly means have been used for the comparison with the model results

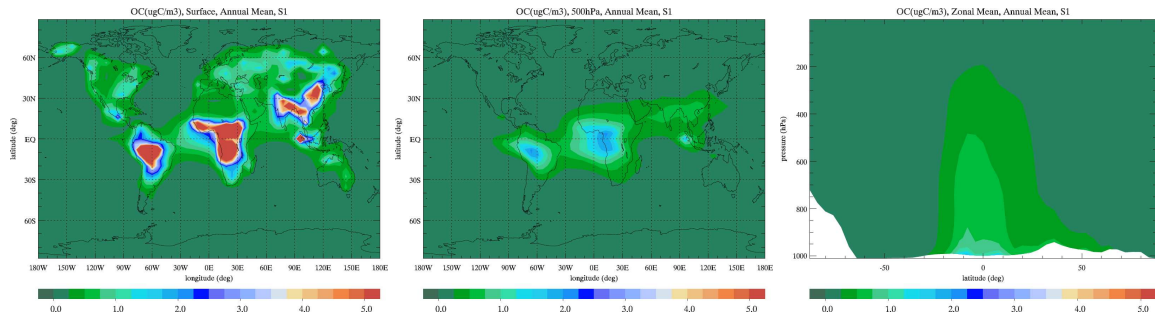
#PTFE : poly Tetra Fluoro ether

Table S4. ANOVA statistics for model evaluation (model versus observations) based on monthly data at specific stations as depicted in Fig. 5 (seasonal) and all data listed in Table S4 on monthly basis as depicted in Fig. 6 (global).

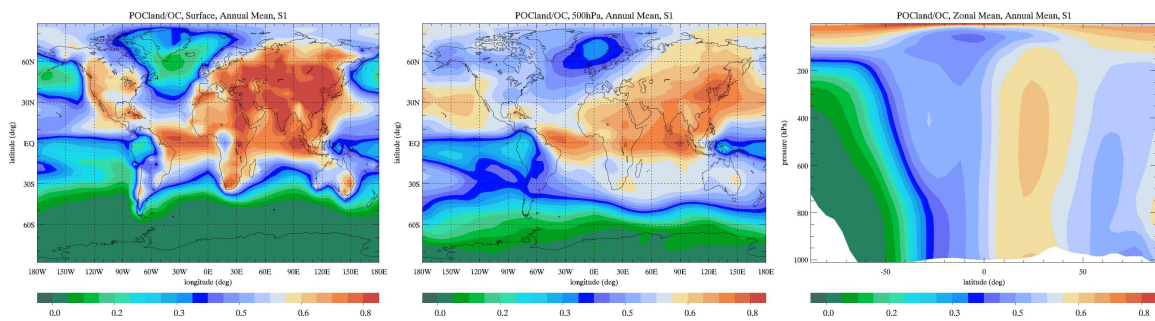
	Station	Simulation	Slope	r^2	N	a	F-value	Prob>F
Global	Urban	S1	0.64±1.19	-0.04	19	0.05	0.290	0.597
	Rural	S1	0.92±0.24	0.18	64	0.05	14.842	2.798 10 ⁻⁴
	Marine	S1	1.13±0.17	0.46	50	0.05	42.653	3.855 10 ⁻⁸
	Rural + Marine	S1	1.16±0.14	0.36	114	0.05	65.598	7.483 10 ⁻¹³
	All Observations	S1	1.29±0.20	0.23	133	0.05	41.346	2.186 10 ⁻⁹
Seasonal	Finokalia	S1	0.72±0.19	0.54	12	0.05	13.779	0.004
		S2	0.73±0.19	0.54	12	0.05	13.805	0.004
		S3	0.95±0.22	0.61	12	0.05	18.124	0.002
		S4	0.96±0.23	0.60	12	0.05	17.247	0.002
	Amsterdam	S1	0.90±0.25	0.52	12	0.05	13.054	0.005
		S2	0.91±0.25	0.53	12	0.05	13.234	0.005
		Island	0.90±0.22	0.59	12	0.05	16.754	0.002
		S4	1.28±0.65	0.21	12	0.05	3.887	0.077
	Mace Head	S1	0.37±0.11	0.50	11	0.05	11.086	0.009
		S2	0.37±0.11	0.50	11	0.05	11.084	0.009
		S3	0.43±0.11	0.60	11	0.05	16.134	0.003
		S4	0.58±0.13	0.63	11	0.05	18.230	0.002
	Aveiro	S1	0.45±0.13	0.50	12	0.05	12.192	0.006
		S2	0.46±0.13	0.51	12	0.05	12.257	0.006
		S3	0.46±0.15	0.44	12	0.05	9.669	0.011
		S4	0.48±0.15	0.46	12	0.05	10.396	0.009
	Azores	S1	0.05±0.09	-0.07	12	0.05	0.292	0.601
		S2	0.06±0.09	-0.07	12	0.05	0.291	0.601
		S3	0.06±0.10	-0.05	12	0.05	0.461	0.512
		S4	0.17±0.13	0.06	12	0.05	1.719	0.219
	Schauinsland	S1	0.35±0.12	0.42	12	0.05	9.007	0.013
		S2	0.34±0.12	0.41	12	0.05	8.715	0.014
		S3	0.21±0.15	0.09	12	0.05	2.071	0.181
		S4	0.22±0.15	0.09	12	0.05	2.111	0.177
	Puy de Dome	S1	0.57±0.12	0.66	12	0.05	22.750	0.001
		S2	0.57±0.12	0.39	12	0.05	22.553	0.001
		S3	0.52±0.13	0.57	12	0.05	15.433	0.003
		S4	0.56±0.14	0.58	12	0.05	16.018	0.002
	K-Pustza	S1	0.01±0.31	-0.10	12	0.05	0.001	0.983
		S2	0.01±0.31	-0.10	12	0.05	0.002	0.964
		S3	0.22±0.25	-0.02	12	0.05	0.825	0.385
		S4	0.23±0.25	-0.01	12	0.05	0.837	0.382

Supplementary Figures:

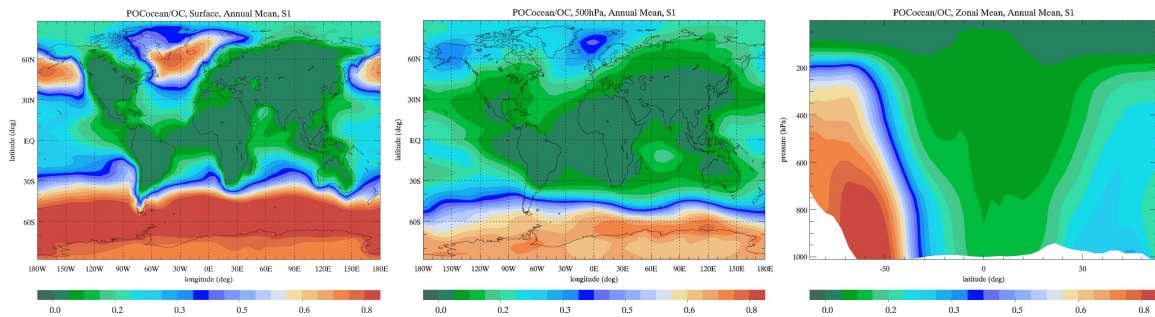
a) OC in $\mu\text{g m}^{-3}$



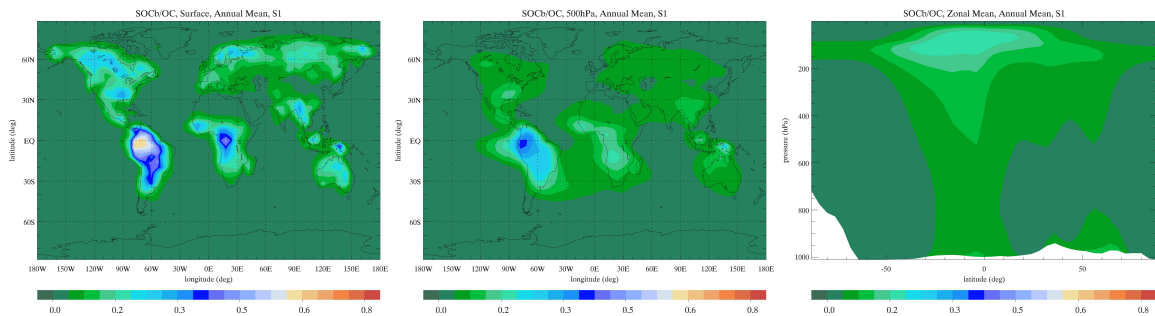
b) $POCl_{land}/OC$



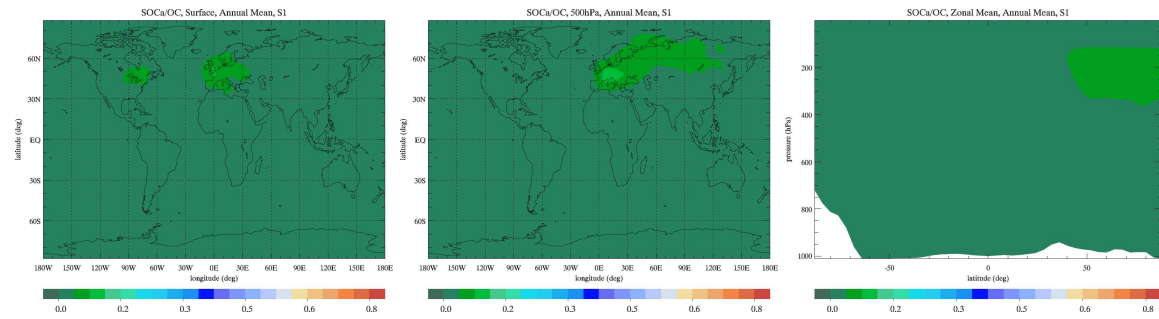
c) $POCocean/OC$



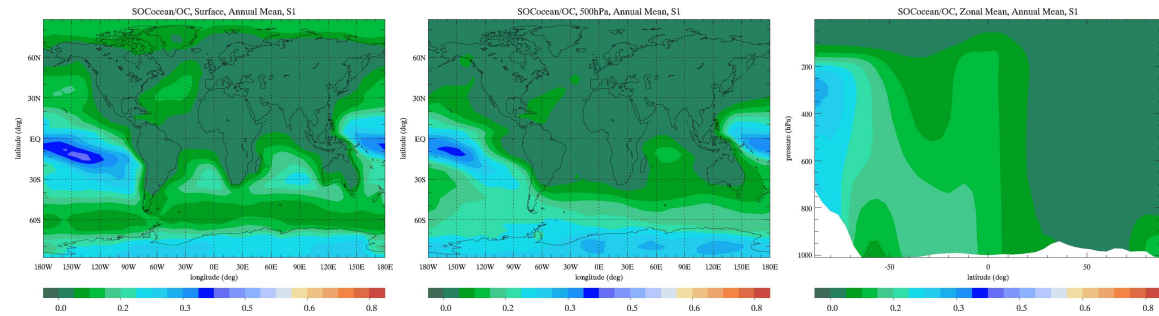
d) $SOCb/OC$



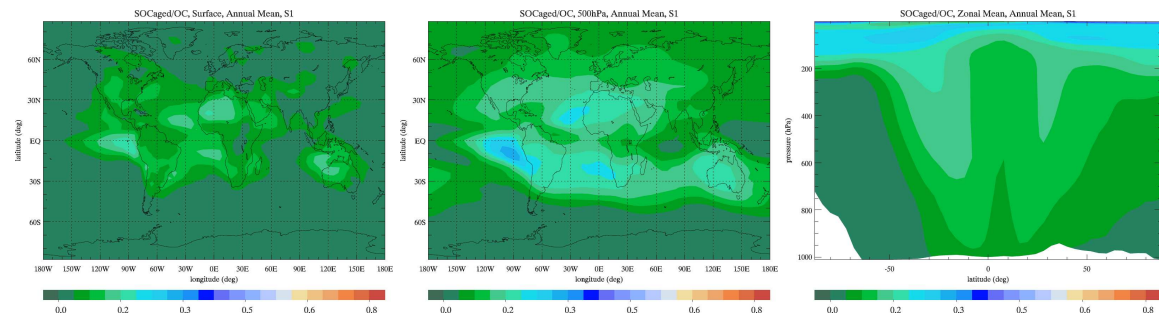
e) $SOCa/OC$



f) SOC_{ocean}/OC



g) SOC_{aged}/OC



h) OC_{oxl}/OC

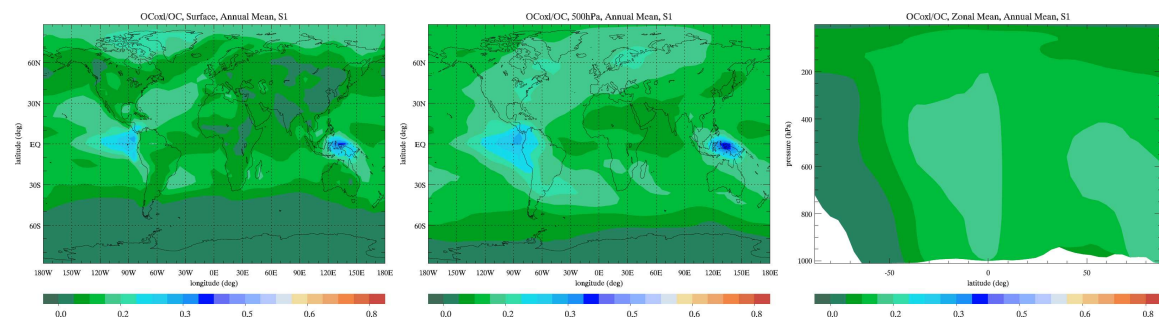


Figure S1. a) Annual mean OC ($\mu\text{gC m}^{-3}$) and annual mean contributions to total OC (carbon mass ratio) of: b) Primary OC from land –POCland, c) Primary OC from oceans – POCocean, d) Secondary OC from precursors of biogenic origin – SOC_b, e) Secondary OC from precursors of anthropogenic origin – SOC_a, f) Secondary OC from precursors of oceanic origin – SOC_{ocean}, g) Aged Secondary OC – SOC_{aged} and h) OXL expressed in carbon mass – OC_{oxl}, as calculated by the model for S1 Simulation; for surface (left), 500 hPa (middle), and zonal mean (right).

Comments relevant to Figure S1:

TM4-ECPL accounts for soluble and insoluble forms of anthropogenic and marine primary OA that is ageing chemically by reaction with O₃ as described in Tsigaridis and Kanakidou (2003). SOA is chemically formed by gas phase oxidation of terpenes and other reactive volatile organics (represented by α- and β- pinenes), isoprene and aromatics (represented by toluene and xylene) and dimethylsulfide. SOA is also allowed to age chemically by reaction with OH radical as in Tsigaridis and Kanakidou (2003). Accounting also for the primary OC and its aged forms we use a total of 19 tracers in our model to simulate organic aerosol components that are grouped in 8 major categories: SOA from anthropogenic volatile organics (SOAa), SOA from biogenic volatile organics (SOAb), methanesulfonic acid (MSA), Marine Amines Salts, Oxalate (OXL), aged SOA, primary OC from fossil fuels, biofuels and biomass burning processes, primary marine OC.

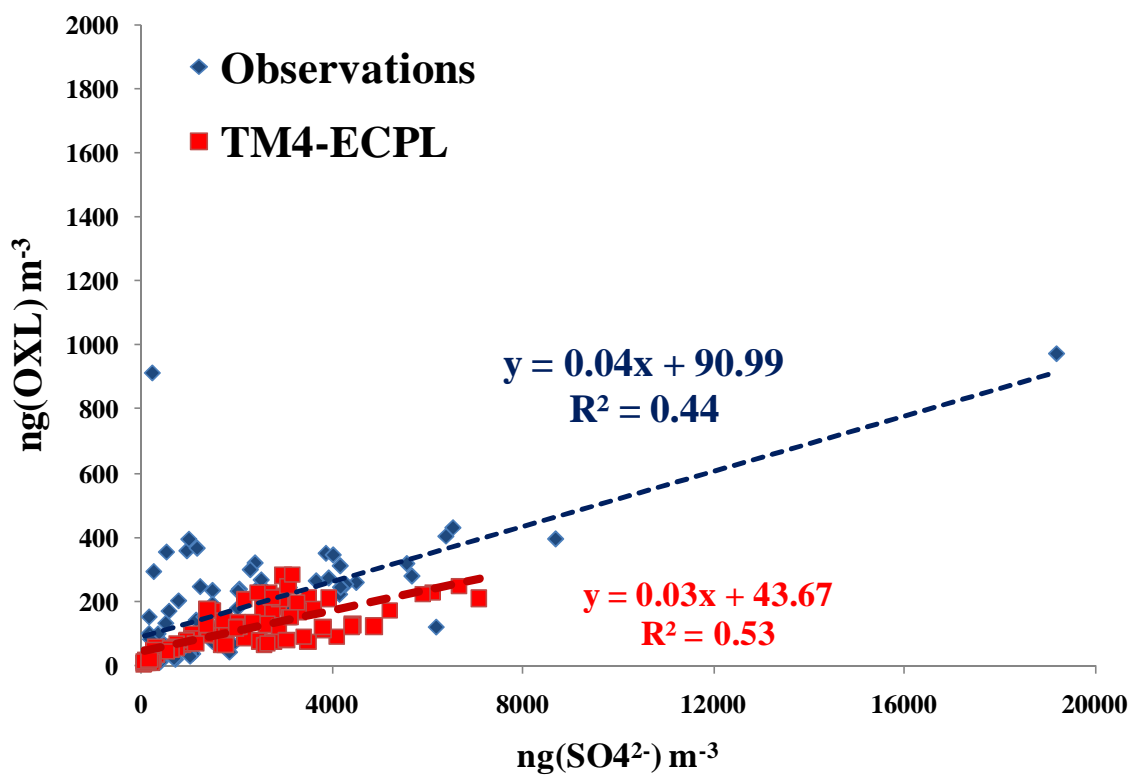


Figure S2. OXL (ng-OXL m⁻³) as a function of SO₄²⁻ (ng-SO₄²⁻ m⁻³) mass concentrations from observations (red squares) and as calculated by the model for S1 Simulation (blue diamonds), based on monthly mean values. Observations are taken from Crahan et al. (2004), Fosco and Schmeling (1988), Biswas et al. (2008), Saarnio et al. (2010), Legrand et al. (2007), Koulouri et al. (2008) and Sciare J. unpublished data.

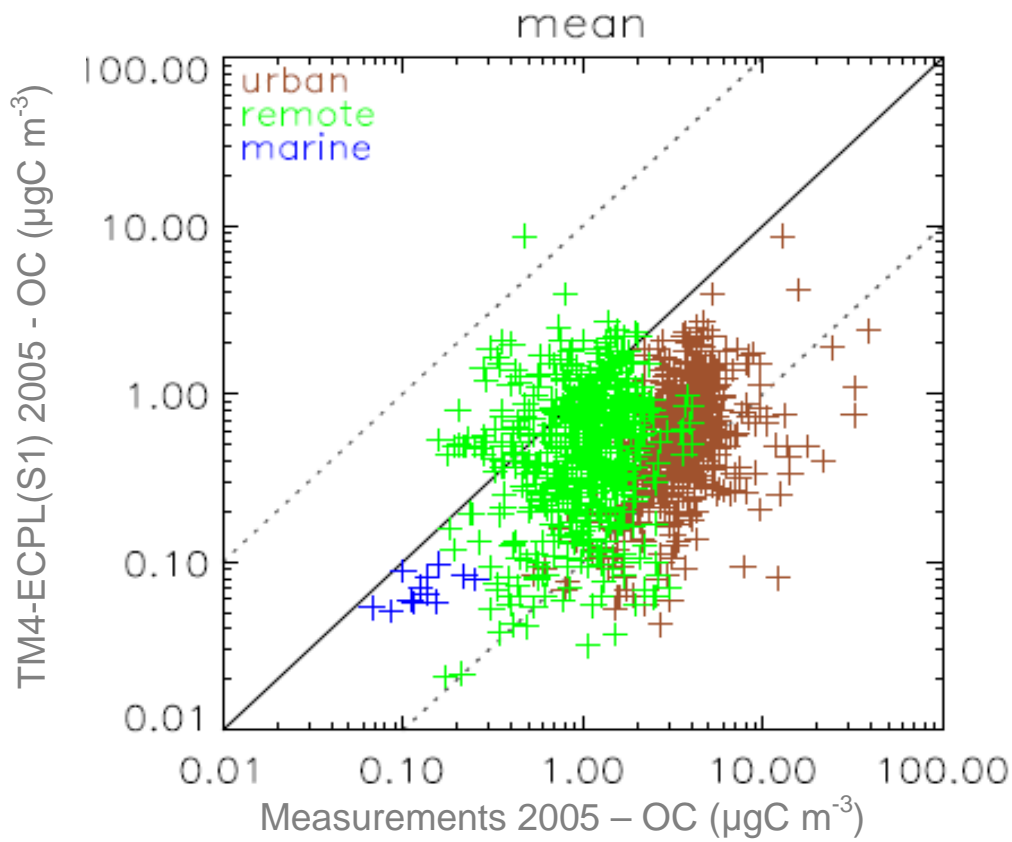
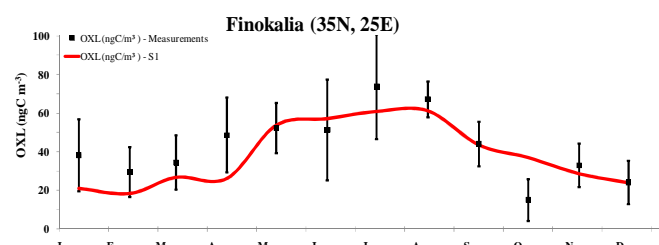
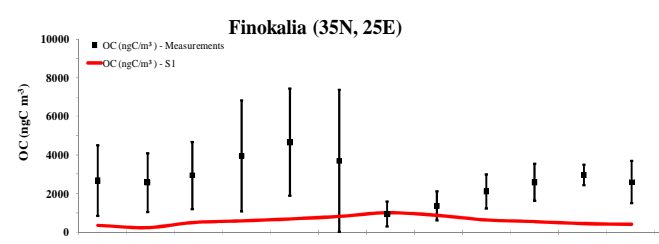
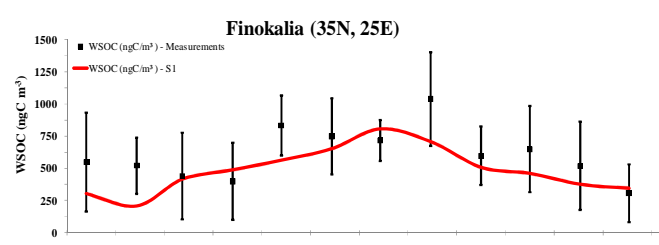
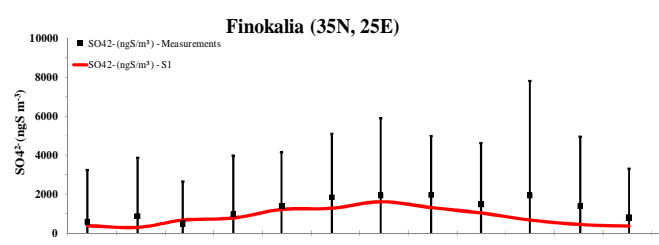
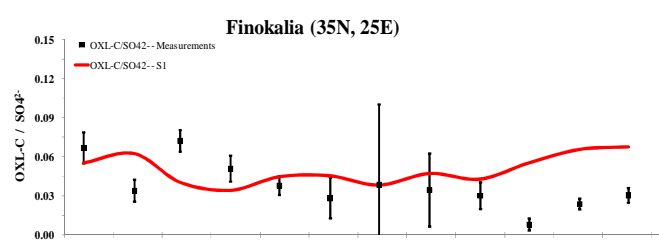
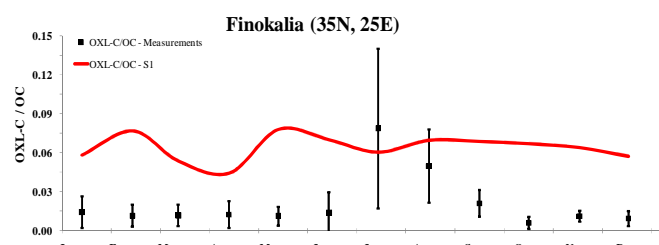
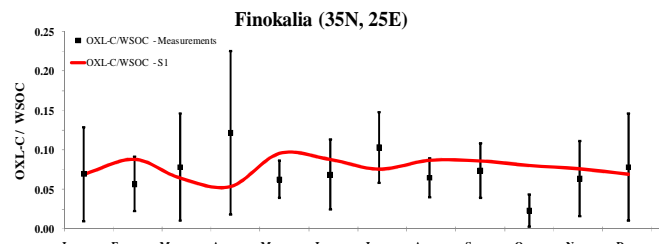
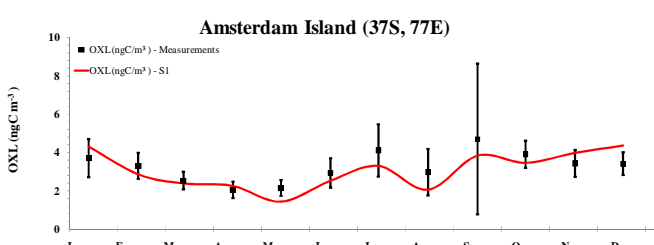
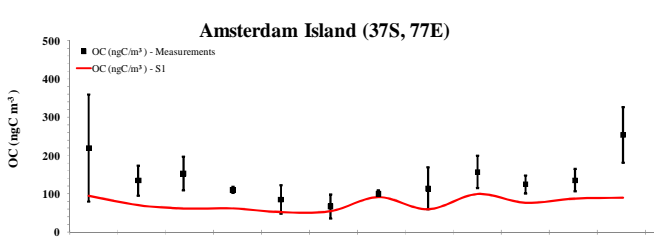
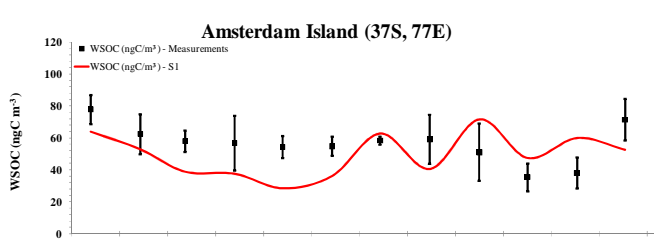
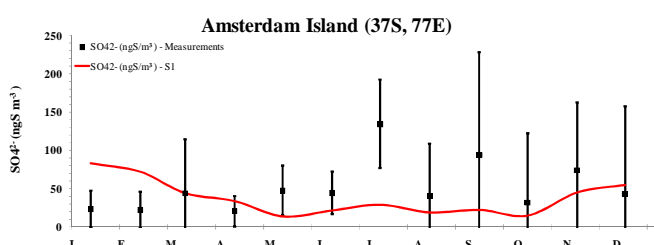
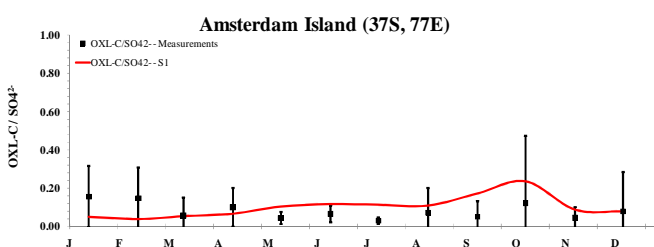
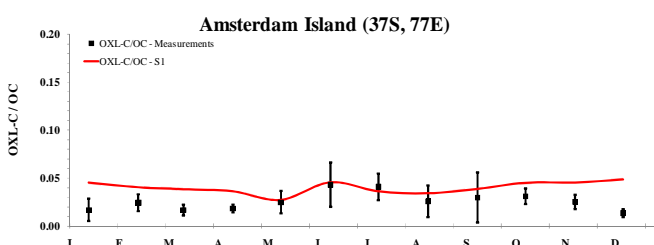
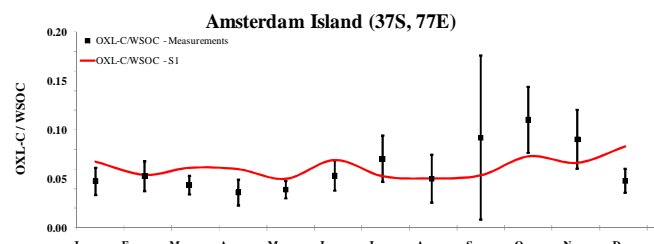
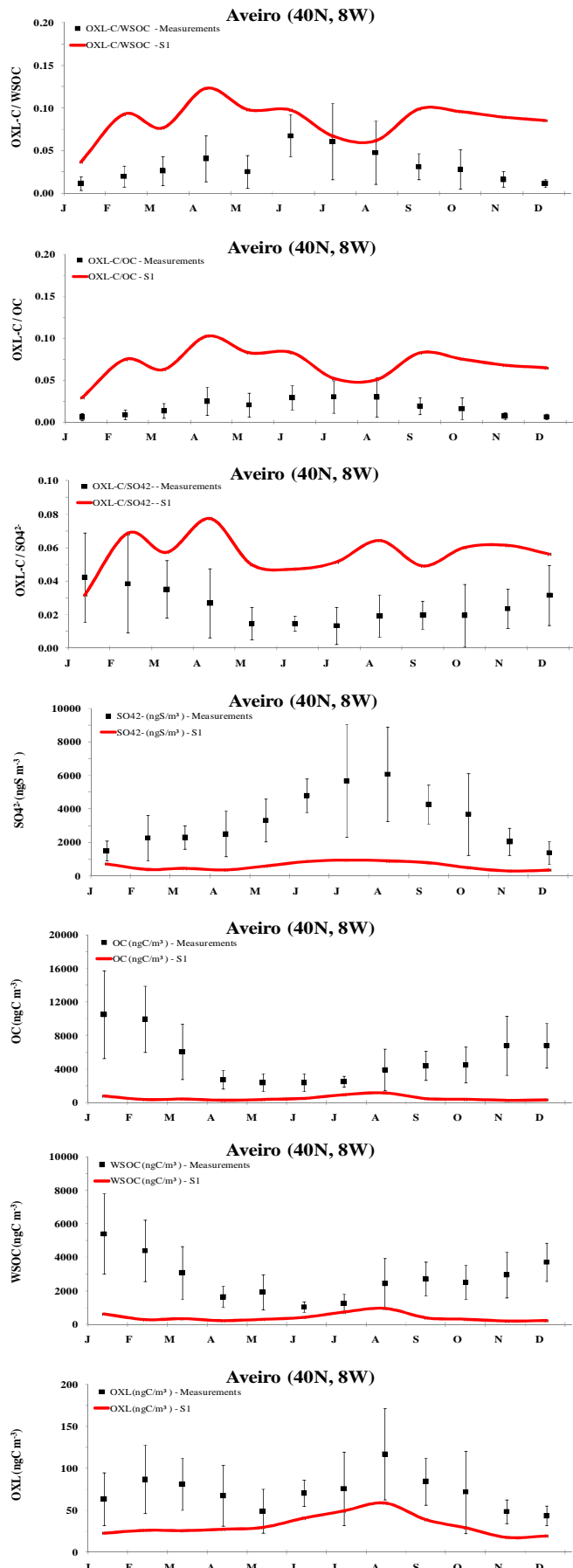


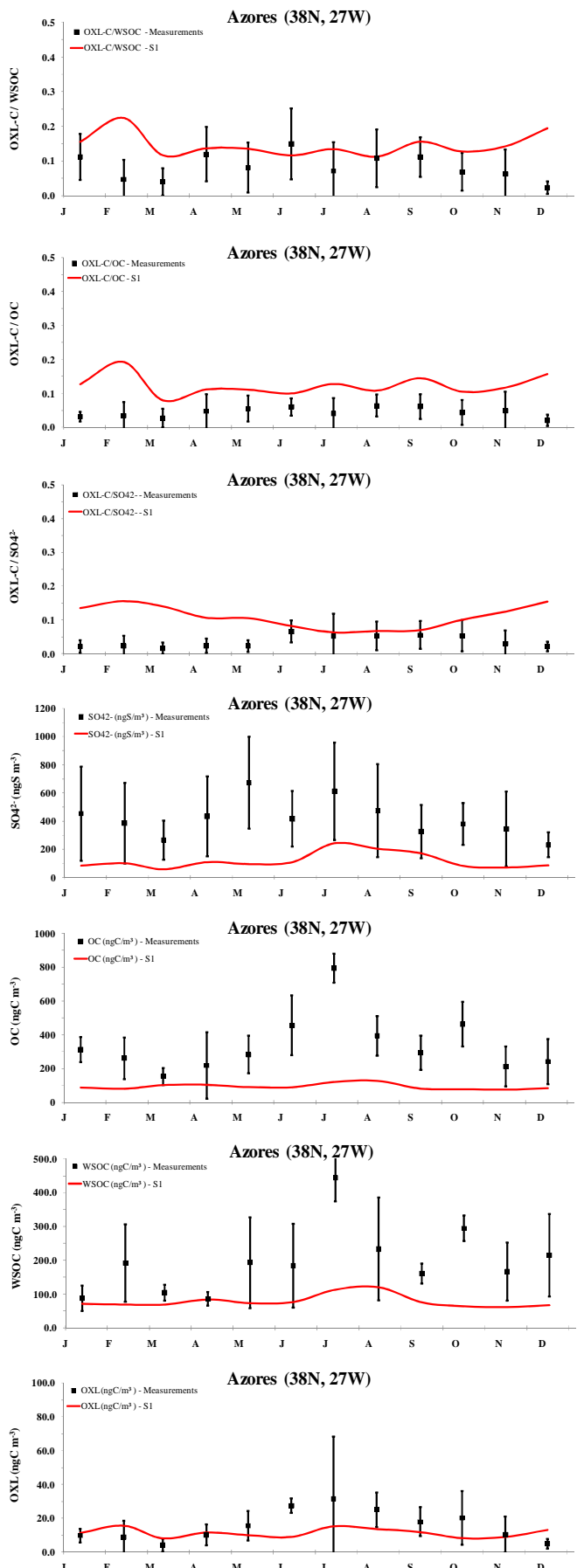
Figure S3. Comparison of OC computed by TM4-ECPL (S1 Simulation) for 2005 (y-axis) with OC - PM2.5 observations (x-axis) in $\mu\text{gC m}^{-3}$ from Bahadur et al. (2009), Sciare et al. (2009) and Koulouri et al. (2008), for urban (brown crosses), remote (green crosses) and marine (blue crosses) locations.

a)**b)**

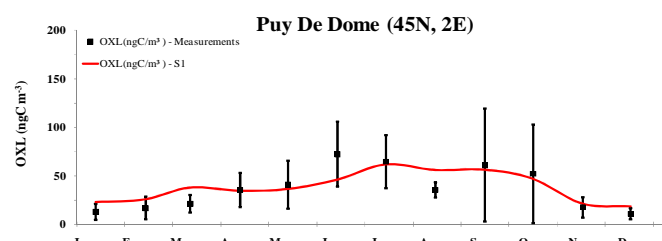
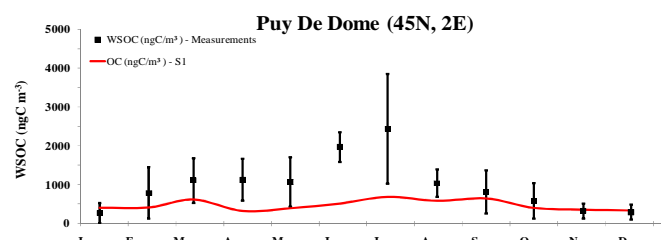
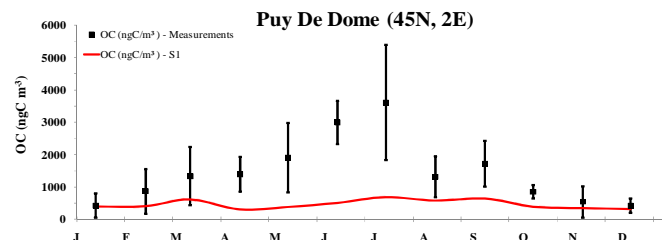
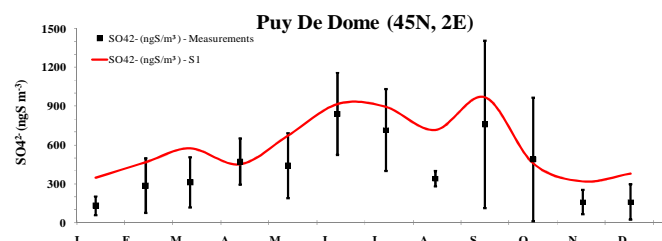
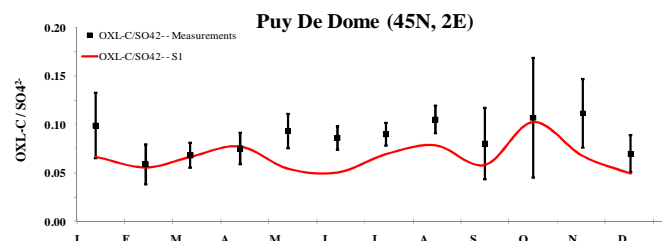
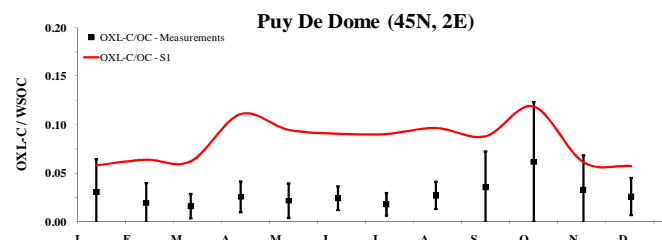
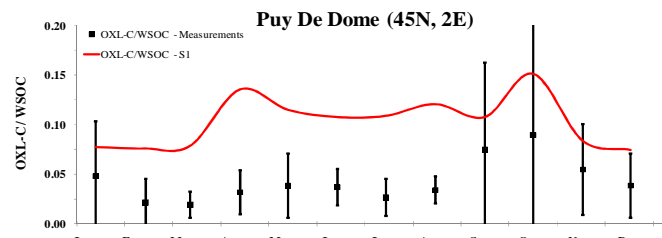
c)



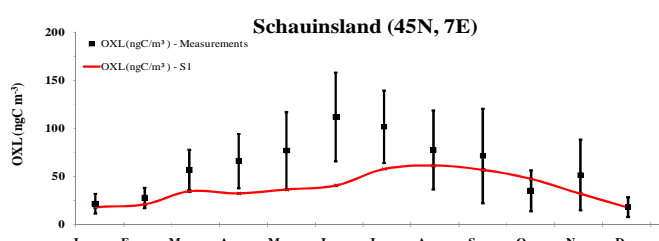
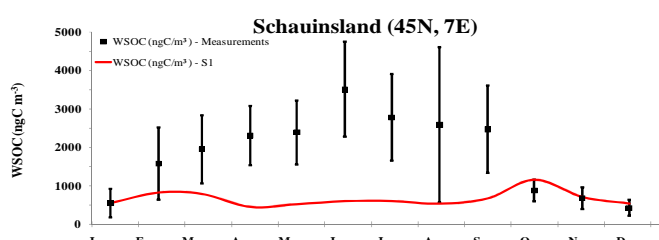
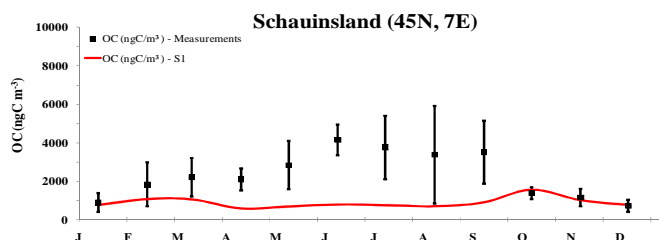
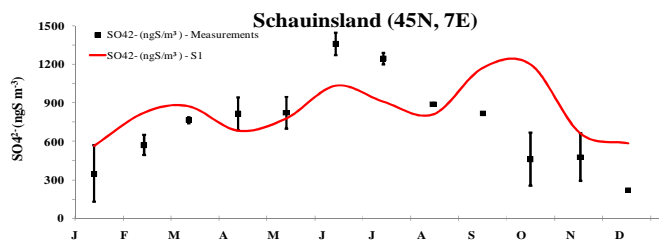
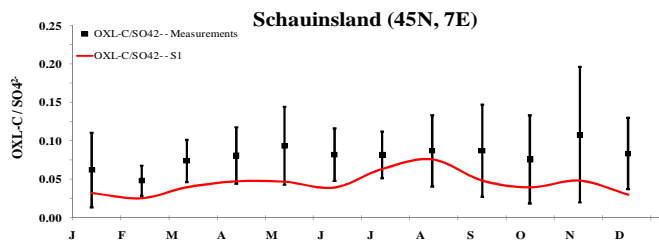
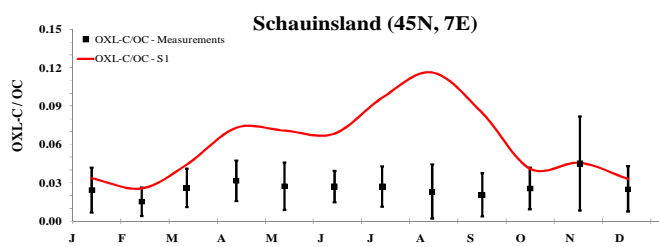
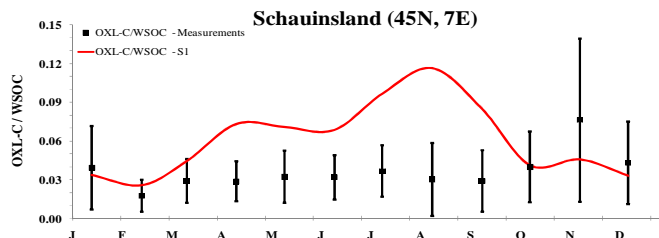
d)



e)



f)



g)

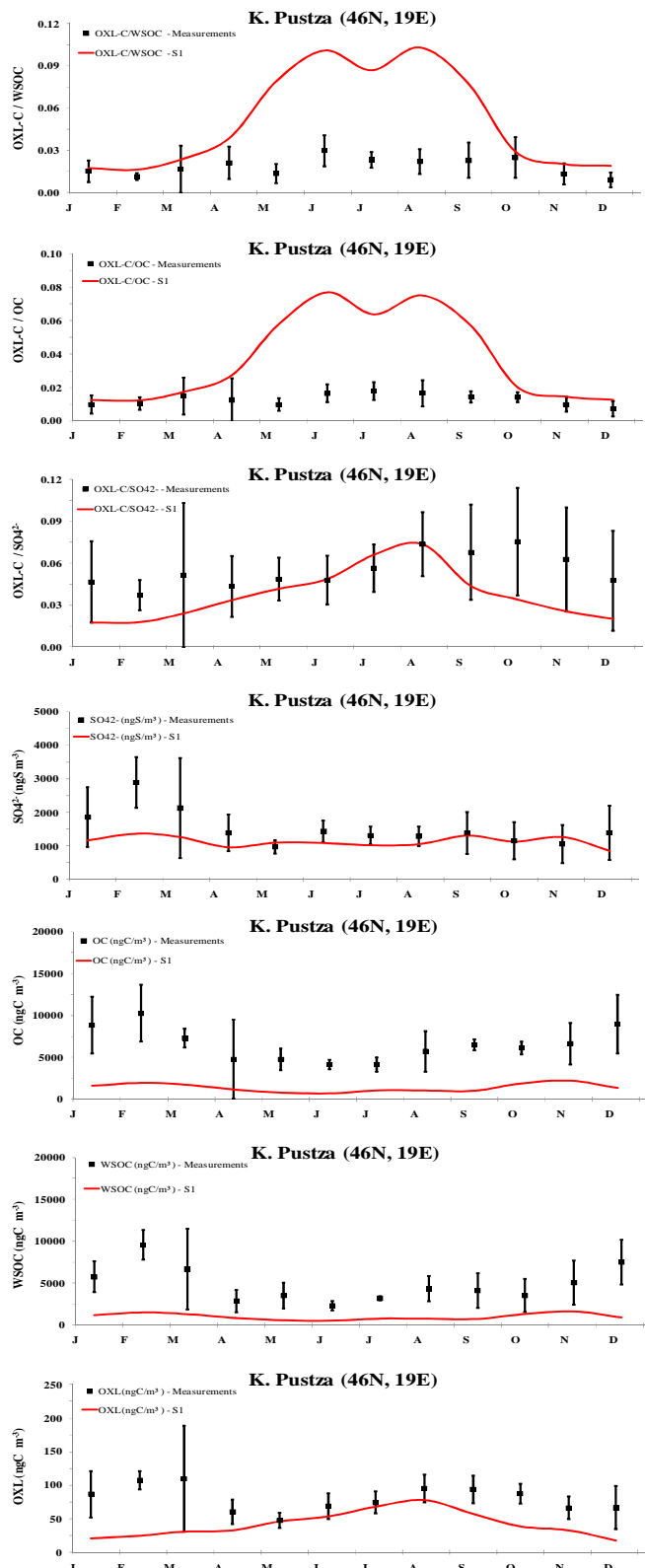


Figure S4. Comparison between model results (S1) (red line) and observations (black squares) of OXL fraction to water soluble organics (OXL/WSOC), to total OC (OXL/OC), to sulfate (OXL/SO₄²⁻) and concentrations of SO₄²⁻, OC, WSOC and OXL (from top to bottom) for the following locations: a) Finokalia, b) Amsterdam Island, c) Aveiro, d) Azores, e) Puy de Dome, f) Schauinsland and g) K-Pustza. All values of organics are expressed in ngC m⁻³; SO₄²⁻ is expressed in ngS m⁻³.

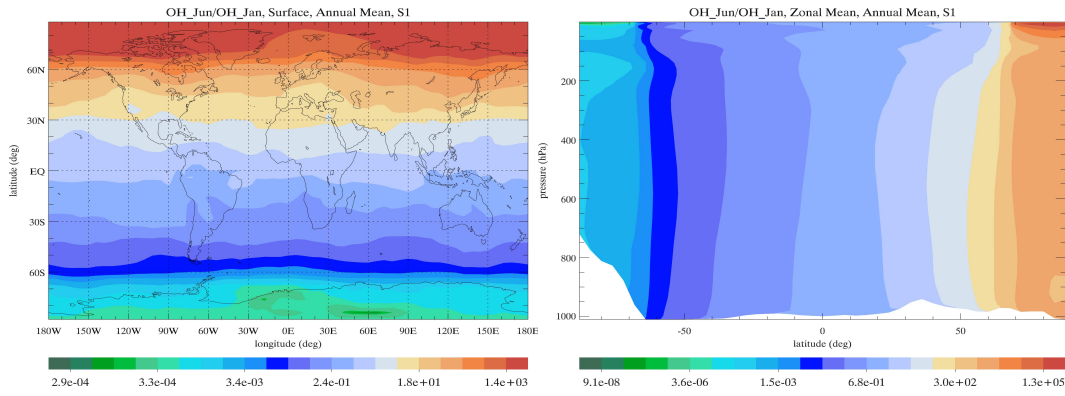


Figure S5: Ratio of OH total concentrations in June to those in January for surface (left panel) and zonal mean (right panel) as calculated by the model for S1 Simulation.

Comments relevant to Figure S5:

TM4-ECPL model output provides the total OH radical concentration (i.e. $\text{OH}_{\text{(tot)}} = \text{OH}_{\text{(g)}} + \text{OH}_{\text{(aq)}}$; see Eq. (4) in section A1) instead of the concentrations in the gas and aqueous phases. Figure S5 depicts the ratio of OH total concentrations in June to those in January for surface and the zonal mean, as calculated by the TM4-ECPL model. Note that, higher biogenic concentrations during summer compete with OH photochemical production, with the net result depending on the location's characteristics.

Hermann et al. (2005) calculated that the most important sources of OH radicals in the droplets are (i) the Fenton reaction between Fe^{2+} and H_2O_2 accounting for about 33%, (ii) the photolytic decomposition of H_2O_2 with a contribution of about 25% and (iii) uptake of OH radicals into the droplets which accounts for about 21% of the total source of OH in the droplets. In TM4-ECPL we account for the last two mechanisms of OH sources in the aqueous phase that are both driven by photochemistry and account for about 63% and 37% of the OH sources in the aqueous-phase, respectively, on an annual basis. Photolysis of NO_3^- and the reaction of $\text{O}_3(\text{aq})$ with O_2^- do not significantly contribute to OH radical formation in the aqueous phase ($\sim 0.11\%$) on an annual basis. It is therefore expected that the aqueous-phase OH radical concentrations are strongly supported by the gas-phase OH concentrations and their transfer to the aqueous-phase.

According to our calculations, the OH radical formation in the aqueous phase in January is by about 2.5% higher than in June on the global scale. This is due to i) a 7.8% higher OH water uptake in January compared to June, which may be attributed to the impact of biogenic emissions on the gas-phase OH radical concentrations during summer, and ii) a 7.3% lower formation of OH radicals in the aqueous-phase by the photolysis of H_2O_2 in January than in June. However, in the Northern Hemisphere, OH aqueous-phase formation is calculated to be more than 2 times higher in June compared to January. The uptake of gas-phase OH radicals in the aqueous phase in June is also enhanced by about 2 times and the production of OH radicals by the H_2O_2 photolysis in the aqueous-phase is calculated to be almost 2.5 times higher than in January.

A1 Exchange between gas and aqueous phase

Aqueous-phase chemistry is simulated in the model as a first-order, first degree homogeneous, ordinary equation:

$$\frac{dC_i}{dt} = P_i - L_i C_i \quad (1)$$

where C_i is the concentration, P_i is the chemical production of the species i , and L_i is the pseudo-first-order loss term of the species i . Because of the stiffness of the simultaneous solution of gaseous and aqueous phase chemistry (lifetime of the species differs by many orders of magnitude), the Euler backward iterative (EBI) method is used, as suggested by Barth et al. (2003). The Barth-EBI approximation is a stable, implicit method which solves Eq. (1) as:

$$C^{n+1,i+1} = \frac{C^n + P^{n=1,i} \Delta t}{1 + L^{n+1,i} \Delta t} \quad (2)$$

where n is the current time step, $n+1$ is the next time step, Δt is the time step duration, and i represents the number of iterations. This method uses 0.01% for the threshold convergence criterion for all species. Important parameters for the solubility of gases in cloud droplets are the liquid water content (LWC) and the temperature (T). The solubility of gases in water is governed by the Henry's law constant (H) (Table S3). For a given T , H and LWC , the phase ratio (Φ_x), which represents the amount of gas in a given volume of air which resides in the aqueous-phase relative to the amount in the interstitial gas-phase (Lelieveld and Crutzen, 1991; Barth et al., 2003), is calculated by:

$$\Phi_x = H(T) \cdot R \cdot T \cdot LWC \quad (3)$$

where, $H(T)$ is the temperature dependent effective Henry's law constant, R is the universal gas constant ($0.0821 \text{ L atm mol}^{-1} \text{ K}^{-1}$), T is the temperature (K) and LWC is the liquid water content ($\text{cm}^3 \text{ H}_2\text{O cm}^{-3} \text{ air}$). The concentration of a species i ($C_{i,liq}$ in molecule cm^{-3}) in the liquid phase in connection with the total concentration (C_{tot} in molecule cm^{-3}) is calculated using Eq. (3) as,

$$C_{i,liq} = \frac{\Phi_x}{1 + \Phi_x} C_{i,tot} \quad (4)$$

However, a chemical species may not achieve equilibrium on the timescales of the model's time step because of mass transfer kinetic limitations between phases (Schwartz, 1986). The rate of change of a chemical species i , due to mass transfer between gas and liquid phase can be defined as:

$$k_{t,i} = \left(\frac{r^2}{3D_g} + \frac{4r}{3va} \right)^{-1} \quad (5)$$

where $k_{t,i}$ is the transfer coefficient (s^{-1}), r the droplet radius (m), D_g the gas-phase diffusion coefficient ($m^2 s^{-1}$), v the mean molecular speed ($m s^{-1}$) and α the mass accommodation coefficient (Table S3). The D_g and the v are defined as:

$$D_g = 1.9(MW)^{-\frac{2}{3}} \quad (6)$$

$$v = \left(\frac{8 k_B T N_a}{\pi (MW)} \right)^{-\frac{1}{2}} \quad (7)$$

where MW is the molecular weight, k_B the Boltzmann constant ($1.38 \cdot 10^{-16} \text{ dyn cm K}^{-1}$) and N_a the Avogadro number ($6.023 \cdot 10^{23} \text{ molecule mol}^{-1}$).

For the present study only OH, HO₂ and NO₃ radicals are considered to be subjected to kinetic limitations. Barth et al. (2003) showed that OH, HO₂ and NO₃ radicals are not in equilibrium between the gas and aqueous phases. For those two radicals, the model calculates the k_t by taking into account mass accommodation coefficients of 0.05, 0.01 and 0.004 for OH, HO₂ and NO₃ radicals respectively, as suggested by Herrmann et al. (2000). Droplet radius varies between $\sim 3.6 - > 16.5 \mu\text{m}$ for remote clouds, 1-15 μm for continental and $\sim 1-25 \mu\text{m}$ for polluted clouds (Herrmann, 2003). For this study we used an average cloud droplet radius of 5 μm over continents, where most of the emission of OXL precursors occurs, and above oceans we used a cloud droplet radius of 10 μm which is more representative for remote clouds. Note, however, that according to Eq. (5), gas transfer to small droplets is faster than to large droplets, which is a result of the larger surface-to-volume ratio of smaller droplets. Although, Lelieveld and Crutzen (1991) suggested that varying droplet sizes does not affect the calculations much, because gas-transfer processes are generally much faster than the chemical processes involved.

References

- Baboukas, E. D., Kanakidou, M., Mihalopoulos, N.: Carboxylic acids in gas and particulate phase above the Atlantic Ocean, *J. Geophys. Res.*, 105, 14459–14471, 2000.
- Bahadur, R., Habib, G., Russell, L. M.: Climatology of PM_{2.5} organic carbon concentrations from a review of ground-based atmospheric measurements by evolved gas analysis, *Atmos. Environ.*, 43, 9, 1591–1602, doi:10.1016/j.atmosenv.2008.12.018, 2009.
- Barth, M. C., Sillman, S., Hudman, R., Jacobson, M. Z., Kim, C.-H., Monod, A., Liang, J.: Summary of the cloud chemistry modeling intercomparison: Photochemical box model simulation, *J. Geophys. Res.*, 108, 4214, doi:10.1029/2002JD002673, 2003.
- Biswas, K. F., Ghauri, B. M., Husain, L.: Gaseous and aerosol pollutants during fog and clear episodes in South Asian urban atmosphere, *Atmos. Environ.*, 42, 7775–7785, 2008.
- Brimblecombe, P., Clegg, S. L., Khan, I.: Thermodynamic properties of carboxylic acids relevant to their solubility in aqueous solutions, *J. Aeros. Sci.*, 23, sup. I, S901-S904, 1992.
- Crahan, K. K., Hegg, D., Covert, D. S., Jonsson H.: An exploration of aqueous oxalic acid production in the coastal marine atmosphere, *Atmos. Environ.* 38, 3757–3764, 2004.
- Falkovich, A. H., Gruber, E. R., Schkolnik, G., Rudich, Y., Maenhaut, W., and Artaxo, P.: Low molecular weight organic acids in aerosol particles from Rondonia, Brazil, during the biomass-burning, transition and wet periods, *Atmos. Chem. Phys.*, 5, 781–797, 2005.
- Fosco, T., and Schmelting, M.: Aerosol ion concentration dependence on atmospheric conditions in Chicago, *Atmos. Environ.* 40, 6638–6649, 2006.
- Graham, B., Mayol-Bracero, O. L., Guyon, P., Roberts, G. C., Decesari, S., Facchini, M. C., Artaxo, P., Maenhaut, W., Koll, P., Andreae, M. O.: Water-soluble organic compounds in biomass burning aerosols over Amazonia – 1. Characterization by NMR and GC-MS, *J. Geophys. Res.*, 107, 8047–8063, doi:10.1029/2001JD000336, 2002.
- Grosjean, D.: Aldehydes, carboxylic acids and inorganic nitrate during nsmcs, *Atmos. Environ.*, 22, 1637–1648, 1988.
- He, N., and Kawamura, K.: Distributions and diurnal changes of low molecular weight organic acids and α -dicarbonyls in suburban aerosols collected at Mangshan, North China, *Geochem. J.*, 44, e17-e22, 2010.
- Herrmann, H.: Kinetics of Aqueous Phase Reactions Relevant for Atmospheric Chemistry, *Chem. Rev.* 2003, 103, 4691-4716, doi: 10.1021/cr020658q, 2003.
- Herrmann, H., Tilgner, A., Barzaghi, P., Majdik, Z., Gligorovski, S., Poulain, L., and Monod, A.: Towards a more detailed description of tropospheric aqueous phase organic chemistry: CAPRAM 3.0., *Atmos. Environ.*, 39, 4351-4363, 2005.
- Ip, H. S. S., Huang, X. H. H., Yu, J. Z.: Effective Henry's law constants of glyoxal, glyoxylic acid, and glycolic acid, *Geophys. Res. Lett.*, 36, L01802, doi:10.1029/2008GL036212, 2009.
- Kawamura, K., Ng, L.-L., Kaplan, I. R.: Determination of Organic Acids (Cl-Cl0) in the Atmosphere, Motor Exhausts and Engine Oils, *Environ. Sci. Tech.*, 19, 1082–1086, 1985.
- Kawamura, K., and Ikushima, K.: Seasonal changes in the distribution of dicarboxylic acids in the urban atmosphere, *Environ. Sci. Technol.*, 27, 2227 – 2235, 1993.
- Kawamura, K., Kasukabe, H., and Barrie, L. A.: Source and reaction pathways of dicarboxylic acids, ketoacids and dicarbonyls in arctic aerosols: One year of observations, *Atmos. Environ.*, 30, 1709–1722, 1996.

- Kawamura, K., Imai, Y., Barrie L. A.: Photochemical production and loss of organic acids in high Arctic aerosols during long-range transport and polar sunrise ozone depletion events, *Atmos. Environ.*, 39, 599–614, 2005.
- Kleefeld, S., Hofferb, A., Krivacsy, Z., Jennings, S. G.: Importance of organic and black carbon in atmospheric aerosols at Mace Head, on the West Coast of Ireland ($53^{\circ}19'N$, $9^{\circ}54'W$), *Atmos. Environ.*, 36, 4479–4490, 2002.
- Koulouri, E., Saarikoski, S., Theodosi, C., Markaki, Z., Gerasopoulos, E., Kouvarakis, G., Makela, T., Hillamo, R., Mihalopoulos, N.: Chemical composition and sources of fine and coarse aerosol particles in the Eastern Mediterranean, *Atmos. Environ.* 42, 6542–6550, 2008.
- Kundu, S., Kawamura, K., Lee, M., Andreae, T. W., Hoffer, A., Andreae, M. O.: Comparison of Amazonian biomass burning and East Asian marine aerosols: Bulk organics, diacids and related compounds, water-soluble inorganic ions, stable carbon and nitrogen isotope ratios, *Low Temp. Sci.*, 68, 89–100, 2010.
- Legrand, M., Preunkert, S., Oliveira, T., Pio, C., Hammer, S., Gelencser, A., Kasper-Giebl, A., Laj, P.: Origin of C₂-C₅ dicarboxylic acids in the European atmosphere inferred from year-round aerosol study conducted at a west-east transect, *J. Geophys. Res.*, doi:10.1029/2006JD008019, 2007.
- Lelieveld, J., and Crutzen, P. J.: The role of clouds in tropospheric photochemistry, *J. Atmos. Chem.*, 12, 229–267, 1991.
- Lewandowski, M., Jaoui, M., Kleindienst, T. E., Offenberg, J. H., Edney, E. O.: Composition of PM_{2.5} during the summer of 2003 in Research Triangle Park, North Carolina, *Atmos. Environ.* 41, 4073–4083, 2007.
- Lim, H. J., Carlton, A. G., and Turpin, B. J.: Isoprene forms secondary organic aerosol through cloud processing: Model simulations, *Environ. Sci. Technol.*, 39, 4441–4446, 2005.
- Limbeck, A., Kraxner, Y., Puxbaum, H.: Gas to particle distribution of low molecular weight dicarboxylic acids at two different sites in central Europe (Austria), *Aeros. Sci.* 36, 991–1005, 2005.
- Limbeck, A., and Puxbaum, H.: Organic acids in continental background aerosols, *Atmos. Environ.* 33, 1847–1852, 1999.
- Martinelango, P. K., Dasgupta, P. K., Al-Horr, R. S.: Atmospheric production of oxalic acid/oxalate and nitric acid/nitrate in the Tampa Bay airshed: Parallel pathways, *Atmos. Environ.* 41, 4258–4269, 2007.
- Miyazaki, Y., Aggarwal, S. G., Singh, K., Gupta, P. K., and Kawamura, K.: Dicarboxylic acids and water-soluble organic carbon in aerosols in New Delhi, India, in winter: Characteristics and formation processes, *J. Geophys. Res.*, 114, D19206, doi:10.1029/2009JD011790, 2009.
- Miyazaki, Y., Kawamura, K., and Sawano M.: Size distributions and chemical characterization of water-soluble organic aerosols over the western North Pacific in summer, *J. Geophys. Res.*, 115, D23210, doi:10.1029/2010JD014439, 2010.
- Muller, K., van Pinxteren, D., Plewka, A., Svrcina, B., Kramberger, H., Hofmann, D., Bachmann, K., Herrmann, H.: Aerosol characterisation at the FEBUKO upwind station Goldlauter (II): Detailed organic chemical characterization, *Atmos. Environ.* 39, 4219–4231, 2005.
- Neususs, C., Gnauk, T., Plewka, A., Herrmann, H., and Quinn, P. K.: Carbonaceous aerosol over the Indian Ocean: OC/EC fractions and selected specifications from size segregated onboard samples, *J. Geophys. Res.*, 107, 8031, doi:10.1029/2001JD000327, 2002.
- Norton, R. B., Roberts, J. M., Huebert, B. J.: Tropospheric oxalate, *Geophys. Res. Lett.*, 10, 517–520, doi:10.1029/GL010i007p00517, 1983.

- Pavuluri, C. M., Kawamura, K., and Swaminathan, T.: Water-soluble organic carbon, dicarboxylic acids, ketoacids, and a-dicarbonyls in the tropical Indian aerosols, *J. Geophys. Res.*, 115, D11302, doi:10.1029/2009JD012661, 2010.
- Plewka, A., Gnauk, T., Bruggemann, E., Herrmann, H.: Biogenic contributions to the chemical composition of airborne particles in a coniferous forest in Germany, *Atmos. Environ.*, 40, 103–115, 2006.
- Ruellan, S., Cachier, H., Gaudichet, A., Masclet, P., Lacaux, J. P.: Airborne aerosols over central Africa during the experiment for regional sources and sinks of oxidants (EXPRESSO), *J. Geophys. Res.*, 104, 30 673–30 690, 1999.
- Sander, R.: Compilation of Henry's Law Constants for Inorganic and Organic Species of Potential Importance in Environmental Chemistry, available at <http://www.mpch-mainz.mpg.de/~sander/res/henry.html>, 1999.
- Saarnio, K., Aurela, M., Timonen, H., Saarikoski S., Teinilä, K., Mäkelä, T., Sofiev, M., Koskinen, J., Aalto, P. P., Kulmala, M., Kukkonen, J., Hillamo, R.: Chemical composition of fine particles in fresh smoke plumes from boreal wild-land fires in Europe, *Sci. of the Tot. Environ.*, 408, 2527–2542, 2010.
- Sciare, J., Favez, O., Sarda-Estève, R., Oikonomou, K., Cachier, H., Kazan, V.: Long-term observations of carbonaceous aerosols in the Austral Ocean atmosphere: Evidence of a biogenic marine organic source, *J. Geophys. Res.*, 114, D15302, doi:10.1029/2009JD011998, 2009.
- Schwartz, S. E.: Mass-transport considerations pertinent to aqueous phase reactions of gases on liquid water clouds, in *Chemistry of Multiphase Atmospheric Systems*, NATO ASI Ser., edited by W. Jaeschke, Springer, Berlin, 1986.
- Sempere, R., and Kawamura, K.: Comparative distributions of dicarboxylic acids and related polar compounds in snow, rain and aerosols from urban atmosphere, *Atmos. Environ.* 28, 449-459, 1994.
- Seinfeld, J. H., and Pandis, S. N.: *Atmospheric Chemistry and Physics: From Air Pollution to Climate Change*, A Wiley-Interscience Pub., USA, 1998.
- Souza, S. R., Vasconcellos, P. C., Carvalho, L. R. F.: Low molecular weight carboxylic acids in an urban atmosphere: Winter measurements in Sao Paulo City, Brazil, *Atmos. Environ.*, 33, 2563-2574, 1999.
- Stone, E. A., Hedman, C. J., Zhou, J., Mieritz, M., Schauer, J. J.: Insights into the nature of secondary organic aerosol in Mexico City during the MILAGRO experiment 2006, *Atmos. Environ.*, 44, 312-319, 2010.
- Talbot, R. W. Andreae M. O., Andreae, T. W., Harriss, R. C.: Regional aerosol chemistry of the Amazon basin during the dry season, *J. Geophys. Res.*, 93, 1499-1508, 1988.
- Topping, D., Coe, H., McFiggans, G., Burgess, R., Allan, J., Alfarra, M. R., Bower, K., Choularton, T. W., Decesari, S., Facchini, M. C.: Aerosol chemical characteristics from sampling conducted on the Island of Jeju, Korea during ACE Asia, *Atmos. Environ.*, 38 2111–2123, 2004.
- Viana, M., Lopez, J. M., Querol, X., Alastuey, A., Garcia-Gacio, D., Blanco-Heras, G., Lopez-Mahia, P., Pineiro-Iglesias, M., Sanz, M. J., Sanz, F., Chi, X., Maenhaut, W.: Tracers and impact of open burning of rice straw residues on PM in Eastern Spain, *Atmos. Environ.*, 42 1941–1957, 2008.
- Wang, G., Kawamura, K., Umemoto, N., Xie, M., Hu, S., and Wang, Z.: Water-soluble organic compounds in PM_{2.5} and size-segregated aerosols over Mount Tai in North China Plain, *J. Geophys. Res.*, 114, D19208, doi:10.1029/2008JD011390, 2009.
- Wang, G., Xie, M., Hu, S., Gao, S., Tachibana, E., and Kawamura, K.: Dicarboxylic acids, metals and isotopic compositions of C and N in atmospheric aerosols from inland China: implications for dust and coal burning emission and secondary aerosol formation, *Atmos. Chem. Phys.*, 10, 6087–6096, 2010.